

Structural Characterization and Reactivity of $\text{UO}_2(\text{salophen})\text{L}$ and $[\text{UO}_2(\text{salophen})]_2$: Dimerization of $\text{UO}_2(\text{salophen})$ Fragments in Noncoordinating Solvents (salophen = *N,N'*-Disalicylidene-*o*-phenylenediaminate, L = *N,N*-Dimethylformamide, Dimethyl Sulfoxide)

Koichiro Takao[†] and Yasuhisa Ikeda*

Research Laboratory for Nuclear Reactors, Tokyo Institute of Technology, 2-12-1-N1-34, O-okayama, Meguro-ku, Tokyo 152-8550, Japan

Received June 30, 2006

The molecular structures of $\text{UO}_2(\text{salophen})\text{L}$ (L = DMF, DMSO) and a uranyl–salophen complex without any unidentate ligands (L) in solid and solution were investigated using single-crystal X-ray analysis and IR, ¹H NMR, and UV–visible absorption spectroscopies. As a result, it was found that the uranyl–salophen complex without L is a racemic dimeric complex, $[\text{UO}_2(\text{salophen})]_2$, in which the $\text{UO}_2(\text{salophen})$ fragments are held together by bridging between one of the phenoxide oxygen atoms in salophen and the uranium in the other $\text{UO}_2(\text{salophen})$ unit. Furthermore, it was spectrophotometrically demonstrated that $[\text{UO}_2(\text{salophen})]_2$ retains its dimeric structure even in the noncoordinating solvents such as CH_2Cl_2 and CHCl_3 and is in equilibrium with $\text{UO}_2(\text{salophen})\text{L}$ $\{2\text{UO}_2(\text{salophen})\text{L} \rightleftharpoons [\text{UO}_2(\text{salophen})]_2 + 2\text{L}\}$. The equilibrium constants and thermodynamic parameters of this equilibrium were evaluated from UV–visible absorption and ¹H NMR spectral changes; $\log K_{\text{dim}} = -2.51 \pm 0.01$ for L = DMF and solvent = CH_2Cl_2 , $\log K_{\text{dim}} = -1.68 \pm 0.02$ for L = DMF and solvent = CHCl_3 , $\log K_{\text{dim}} = -4.23 \pm 0.01$ for L = DMSO and solvent = CH_2Cl_2 , and $\log K_{\text{dim}} = -3.03 \pm 0.02$ for L = DMSO and solvent = CHCl_3 . The kinetics of L-exchange reactions in $\text{UO}_2(\text{salophen})\text{L}$ and enantiomer exchange of $[\text{UO}_2(\text{salophen})]_2$ in noncoordinating solvents were also studied using NMR line-broadening method. As a consequence, it was suggested that the DMF-exchange reaction in $\text{UO}_2(\text{salophen})\text{DMF}$ proceeds through two pathways (*dissociative* and *associative* paths) and that the predominant path of DMSO exchange in $\text{UO}_2(\text{salophen})\text{DMSO}$ is the dissociative one. A sliding motion of the $\text{UO}_2(\text{salophen})$ fragments was considered to be reasonable for the enantiomer-exchange mechanism of $[\text{UO}_2(\text{salophen})]_2$. On the basis of the kinetic information for $\text{UO}_2(\text{salophen})\text{L}$ and $[\text{UO}_2(\text{salophen})]_2$, reaction mechanisms including the L-exchange reaction in $\text{UO}_2(\text{salophen})\text{L}$, the formation of $[\text{UO}_2(\text{salophen})]_2$ from $\text{UO}_2(\text{salophen})\text{L}$, and the enantiomer exchange of $[\text{UO}_2(\text{salophen})]_2$ are proposed.

1. Introduction

N,N'-Disalicylidene-*o*-phenylenediaminate (salophen), which is one of the most popular tetradentate Schiff base ligands, forms complexes with various metal ions including the hexavalent uranyl ion (UO_2^{2+}).^{1,2} Generally, the uranyl complexes with salophen and its derivatives have a pentagonal-

bipyramidal geometry, i.e., the equatorial plane of the uranyl ion is coordinated by salophen and a unidentate ligand (L). For instance, the molecular structure of the ethanol adduct $\text{UO}_2(\text{salophen})\text{EtOH}$ was reported by Bandoli et al.³ They pointed out that the stability of $\text{UO}_2(\text{salophen})\text{L}$ depends on L [$\text{Ph}_3\text{PO} > \text{dimethyl sulfoxide (DMSO)} > \text{pyridine} \geq \text{aniline} > \text{EtOH}$].

Recently, many attempts have been made to apply such differences in the stability of $\text{UO}_2(\text{salophen})\text{L}$ and its derivatives to molecular recognition of urea derivatives,^{4–7}

* Corresponding author. E-mail: yiked@nr.titech.ac.jp. Phone and fax: +81-3-5734-3061.

[†] This author's last name was changed from "Mizuoka".

(1) In this article, the oxidation number of uranium in "uranyl" ion is 6, if any indication is not presented.

(2) Pfeiffer, P.; Hesse, T.; Pfitzner, H.; Scholl, W.; Thielert, H. *J. Prakt. Chem.* **1937**, *149*, 217–296.

(3) Bandoli, G.; Clemente, D. A.; Croatto, U.; Vidali, M.; Vigato, P. A. *Chem. Commun.* **1971**, 1330–1331.

pyridine derivatives, amines, quinolines, nitriles,^{8,9} and anions (H_2PO_4^- , Cl^- , NO_2^- , and so on)^{10–20} and to use these materials as catalysts for acyl transfer²¹ and Michael-type addition of thiols.^{22–25} In these functionalities of the uranyl–salophen derivatives, the fifth equatorial coordination site in the $\text{UO}_2(\text{salophen})$ unit plays the most important role as the recognition or activation site of the substrate. As reactants, uranyl–salophen complexes have frequently been treated as the L-dissociated form. However, the molecular structure of such a uranyl–salophen complex with the vacant coordination site has not yet been determined.

Previously, we studied electrochemical reductions of $\text{UO}_2(\text{salophen})\text{L}$ [L = *N,N*-dimethylformamide (DMF), DMSO] and found that the electrochemically generated $[\text{U}^{\text{VO}}_2(\text{salophen})\text{L}]^-$ complexes release L to form $[\text{U}^{\text{VO}}_2(\text{salophen})]^-$.²⁶ This phenomenon was demonstrated by the L concentration dependence of the cyclic voltammogram of $\text{UO}_2(\text{salophen})\text{L}$ in mixed solvents of CH_2Cl_2 and L. With a decrease in the concentration of L in CH_2Cl_2 , the dissociation of L was found to be enhanced. In the $[\text{U}^{\text{VO}}_2(\text{salophen})\text{DMF}]^-/\text{U}^{\text{VI}}\text{O}_2(\text{salophen})\text{DMF}$ redox couple, DMF dissociation

from $[\text{U}^{\text{VO}}_2(\text{salophen})\text{DMF}]^-$ occurs even in the neat DMF solvent. It was confirmed that the dissociation of L changes the oxidation potential of the center uranium(V) by ca. 0.5 V. Therefore, it can be expected that chemical properties of uranyl(VI)–salophen complexes without L also differ from those of $\text{UO}_2(\text{salophen})\text{L}$.

Furthermore, Comyns et al. reported an interesting phenomenon for $\text{UO}_2(\text{acac})_2\text{OH}_2$ (acac = acetylacetonate).²⁷ According to them, solutions of $\text{UO}_2(\text{acac})_2\text{OH}_2$ in noncoordinating solvents (benzene, chlorobenzene, and dichloroethane) became redder on heating, whereas those in coordinating solvents (ethanol, *n*-pentyl acetate, and cyclohexanone) did not show such a phenomenon. They also found that the molecular weight of anhydrous $\text{UO}_2(\text{acac})_2$ complex in benzene at 80 °C is that of a dimer, $[\text{UO}_2(\text{acac})_2]_2$, and suggested that the dimeric compound in benzene is formed by coordination of the acac oxygen atoms to the adjacent uranium atoms. However, no structural information on such a uranyl–acac dimer has been obtained experimentally.

The previous results on $[\text{U}^{\text{VO}}_2(\text{salophen})\text{L}]^-$ and $\text{UO}_2(\text{acac})_2$ complexes provided the following insights: (i) L dissociation from $\text{UO}_2(\text{salophen})\text{L}$ might occur in the noncoordinating solvents, and (ii) the uranyl–salophen complex without L might prefer a dimeric structure connected by bridging between the $\text{UO}_2(\text{salophen})$ units instead of the monomeric complex with a vacant site. In this study, we have investigated the chemical behavior of $\text{UO}_2(\text{salophen})\text{L}$ in CH_2Cl_2 and CHCl_3 solutions²⁸ and attempted to elucidate the molecular structure of the uranyl–salophen complex without L in the solid and in solution by using single-crystal X-ray analysis and IR, ¹H NMR, and UV–visible absorption spectroscopies.

2. Experimental Section

Materials. The mononuclear complexes $\text{UO}_2(\text{salophen})\text{L}$ (L = DMF, DMSO) were prepared by the method described in a previous article.²⁶ Crystals of $\text{UO}_2(\text{salophen})\text{DMF}$ (**1**) suitable for the X-ray crystallography were obtained by recrystallization from a mixed solvent of CH_2Cl_2 and DMF, and those of $\text{UO}_2(\text{salophen})\text{DMSO}$ (**2**) were obtained from a DMSO solution. The dinuclear complex $[\text{UO}_2(\text{salophen})]_2$ (**3**) was synthesized by dissolving $\text{UO}_2(\text{salophen})\text{L}$ in CH_2Cl_2 , followed by evaporating the solvent slowly. The resulting red crystals of **3** were suitable for the X-ray crystallography. Dichloromethane and CHCl_3 were purified by dehydration using CaH_2 and distillation. *N,N*-Dimethylformamide and DMSO were distilled in vacuo after stirring with CaH_2 . After purification, these solvents were stored over molecular sieves 4A. Deuterated dichloromethane (CD_2Cl_2 , Acros, 99.8 atom % D) and chloroform (CDCl_3 , Acros, 99.8 atom % D) for the NMR measurements were used as received. All other commercially available chemicals were of reagent grade and were used without further purification.

IR data (KBr , cm^{-1}). $\text{UO}_2(\text{salophen})\text{DMF}$ (**1**): 905 (O=U=O asymmetric stretching, ν_3), 1609 (C=N stretching in salophen, $\nu_{\text{C=N}}$)

- (4) van Staveren, C. J.; Fenton, D. E.; Reinhoudt, D. N.; van Eerden, J.; Harkema, S. *J. Am. Chem. Soc.* **1987**, *109*, 3456–3458.
- (5) van Staveren, C. J.; van Eerden, J.; van Veggel, F. C. J. M.; Harkema, S.; Reinhoudt, D. N. *J. Am. Chem. Soc.* **1988**, *110*, 4994–5008.
- (6) van Doorn, A. R.; Rushton, D. J.; W. Verboom, van Straaten-Nijenhuisand W.; Reinhoudt, D. N. *Recl. Trav. Chim. Pays-Bas* **1992**, *111*, 421–426.
- (7) van Straaten-Nijenhuis, W. F.; van Doorn, A. R.; Reichwein, A. M.; de Jong, F.; Reinhoudt, D. N. *J. Org. Chem.* **1993**, *58*, 2265–2271.
- (8) van Doorn, A. R.; Bos, M.; Harkema, S.; van Eerden, J.; Verboom, W.; Reinhoudt, D. N. *J. Org. Chem.* **1991**, *56*, 2371–2380.
- (9) van Doorn, A. R.; Rushton, D. J.; Bos, M.; Verboom, W.; Reinhoudt, D. N. *Recl. Trav. Chim. Pays-Bas* **1992**, *111*, 415–420.
- (10) Rudkevich, D. M.; Verboom, W.; Brzozka, Z.; Palys, M. J.; Stauthamer, W. P. R. V.; van Hummel, G. J.; Franken, S. M.; Harkema, S.; Engbersen, J. F. J.; Reinhoudt, D. N. *J. Am. Chem. Soc.* **1994**, *116*, 4341–4351.
- (11) Verboom, W.; Rudkevich, D. M.; Reinhoudt, D. N. *Pure Appl. Chem.* **1994**, *66*, 679–686.
- (12) Antonisse, M. M. G.; Snellink-Ruël, B. H. M.; Yigit, I.; Engbersen, J. F. J.; Reinhoudt, D. N. *J. Org. Chem.* **1997**, *62*, 9034–9038.
- (13) Antonisse, M. M. G.; Snellink-Ruël, B. H. M.; Engbersen, J. F. J.; Reinhoudt, D. N. *J. Org. Chem.* **1998**, *63*, 9776–9781.
- (14) Antonisse, M. M. G.; Snellink-Ruël, B. H. M.; Ion, A. C.; Engbersen, J. F. J.; Reinhoudt, D. N. *J. Chem. Soc., Perkin Trans. 2* **1999**, 1211–1218.
- (15) Antonisse, M. M. G.; Reinhoudt, D. N. *Chem. Commun.* **1998**, 443–448.
- (16) Cametti, M.; Nissinen, M.; Dalla Cort, A.; Mandolini, L.; Rissanen, K. *Chem. Commun.* **2003**, 2420–2421.
- (17) Dalla Cort, A.; Murua, J. I. M.; Pasquini, C.; Pons, M.; Schiaffino, L. *Chem. Eur. J.* **2004**, *10*, 3301–3307.
- (18) Cametti, M.; Nissinen, M.; Dalla Cort, A.; Mandolini, L.; Rissanen, K. *J. Am. Chem. Soc.* **2005**, *127*, 3831–3837.
- (19) Wojciechowski, K.; Wróblewski, W.; Brzózka, Z. *Anal. Chem.* **2003**, *75*, 3270–3273.
- (20) Brynda, M.; Wesolowski, T. A.; Wojciechowski, K. *J. Phys. Chem. A* **2004**, *108*, 5091–5099.
- (21) van Axel Castelli, V.; Cacciapaglia, R.; Chiosis, G.; van Veggel, F. C. J. M.; Mandolini, L.; Reinhoudt, D. N. *Inorg. Chim. Acta* **2996**, *246*, 181–193.
- (22) van Axel Castelli, V.; Dalla Cort, A.; Mandolini, L. *J. Am. Chem. Soc.* **1998**, *120*, 12688–12689.
- (23) van Axel Castelli, V.; Bernardi, F.; Dalla Cort, A.; Mandolini, L.; Rossi, I.; Schiaffino, L. *J. Org. Chem.* **1999**, *64*, 8122–8126.
- (24) van Axel Castelli, V.; Dalla Cort, A.; Mandolini, L.; Reinhoudt, D. N.; Schiaffino, L. *Chem. Eur. J.* **2000**, *6*, 1193–1198.
- (25) van Axel Castelli, V.; Dalla Cort, A.; Mandolini, L.; Reinhoudt, D. N.; Schiaffino, L. *Eur. J. Org. Chem.* **2003**, 627–633.
- (26) Mizuoka, K.; Kim, S.-Y.; Hasegawa, M.; Hoshi, T.; Uchiyama, G.; Ikeda, Y. *Inorg. Chem.* **2003**, *42*, 1031–1038.

(27) Comyns, A. E.; Gatehouse, B. M.; Wait, E. *J. Chem. Soc.* **1958**, 4655–4665.

(28) These solvents were selected for sufficient solubility of the uranyl–salophen complexes.

Table 1. Crystallographic Data of Uranyl–Salophen Complexes

	UO ₂ (salophen)DMF·CH ₂ Cl ₂	UO ₂ (salophen)DMSO	[UO ₂ (salophen)] ₂	[UO ₂ (salophen)] ₂ ·0.5CH ₂ Cl ₂
abbreviation	1 ·CH ₂ Cl ₂	2	3	3 ·0.5CH ₂ Cl ₂
empirical formula	C ₂₄ H ₂₃ Cl ₂ N ₃ O ₅ U	C ₂₂ H ₂₀ N ₂ O ₅ SU	C ₄₀ H ₂₈ N ₄ O ₈ U ₂	C _{40.5} H ₂₉ ClN ₄ O ₈ U ₂
formula weight	742.38	662.49	1168.72	1211.19
crystal system	monoclinic	monoclinic	triclinic	triclinic
space group	<i>P</i> 2 ₁ / <i>n</i> (No. 14)	<i>P</i> 2 ₁ (No. 4)	<i>P</i> $\bar{1}$ (No. 2)	<i>P</i> $\bar{1}$ (No. 2)
<i>a</i> (Å)	10.667(4)	13.303(7)	15.689(7)	15.717(5)
<i>b</i> (Å)	9.608(3)	9.422(4)	16.044(5)	15.993(7)
<i>c</i> (Å)	24.86(1)	17.205(8)	17.642(7)	17.619(5)
α (deg)			67.00(3)	67.45(3)
β (deg)	100.65(3)	94.45(5)	78.25(3)	77.99(3)
γ (deg)			81.72(3)	81.66(3)
<i>V</i> (Å ³)	2504(2)	2150(2)	3992(3)	3990(2)
<i>Z</i>	4	4	4	4
temperature (K)	123	113	93	93
<i>D</i> _{calcd} (g·cm ⁻³)	1.969	2.047	1.945	2.016
<i>F</i> ₀₀₀	1416	1256	2176	2260
2 θ _{max} (deg)	54.96	54.98	54.96	54.96
observed data (all)	5734	9110	17643	17850
<i>R</i> ^a (<i>I</i> > 2 σ)	0.0258	0.0267	0.0578	0.0594
<i>R</i> _w ^b (all)	0.0650	0.0677	0.1082	0.1297
GOF ^c	1.119	1.088	1.022	1.031
residue (e Å ⁻³) ^d				
maximum	0.964	0.955	1.726	2.490
minimum	-0.740	-0.918	-2.211	-2.984

^a $R = \sum ||F_o| - |F_c|| / \sum |F_o|$. ^b $R_w = [\sum (w(F_o^2 - F_c^2)^2) / \sum w(F_o^2)^2]^{1/2}$. ^c $GOF = [\sum w(F_o^2 - F_c^2)^2 / (N_o - N_v)]^{1/2}$. Detailed values of the weight (*w*) in each system are given in the crystallographic information file provided as Supporting Information. ^d Maximum and minimum residual peaks on the final difference Fourier map for each crystal.

N), and 1651 (C=O stretching in DMF, $\nu_{C=O}$). UO₂(salophen) DMSO (**2**): 897 (ν_3), 999 (S=O stretching in DMSO, $\nu_{S=O}$), and 1605 ($\nu_{C=N}$). [UO₂(salophen)]₂ (**3**): 920 (ν_3) and 1606 ($\nu_{C=N}$).

Methods. Characterizations of the complexes **1–3** were performed using an IR spectrophotometer (Shimadzu FTIR-8400S), an NMR spectrometer (JEOL JNM-LA300WB FT NMR system; ¹H, 300.4 MHz; reference, TMS), a UV–visible spectrophotometer (Shimadzu UV-3150), and a single-crystal X-ray diffractometer (Rigaku RAXIS RAPID).

Single-crystal X-ray analyses of crystals of UO₂(salophen)DMF·CH₂Cl₂ (**1**·CH₂Cl₂), UO₂(salophen)DMSO (**2**), [UO₂(salophen)]₂ (**3**), and [UO₂(salophen)]₂·0.5CH₂Cl₂ (**3**·0.5CH₂Cl₂) were performed by the following procedure: A single crystal of each uranyl complex was mounted on a glass fiber and placed under a low-temperature nitrogen gas flow. Intensity data were collected using imaging plate area detector in the single-crystal X-ray diffractometer with graphite-monochromated Mo K α radiation ($\lambda = 0.71075$ Å). The structures of these uranyl complexes were solved by direct (SIR 92)²⁹ or heavy-atom Patterson methods³⁰ and expanded using Fourier techniques.³¹ All non-hydrogen atoms were anisotropically refined using SHELXL-97.³² Hydrogen atoms were refined using the riding model (C–H bond; aromatic, 0.95 Å; methyl, 0.98 Å). The final cycle of full-matrix least-squares refinement on *F*² was based on observed reflections and parameters and converged with unweighted and weighted agreement factors, *R* and *R*_w. All calculations were performed with the CrystalStructure crystallographic software

package.³³ Crystal data and other data collection parameters are summarized in Table 1. Crystallographic information files for the uranyl–salophen complexes are available as Supporting Information.

The dependence of the UV–visible absorption spectrum of complex **3** on L concentration was recorded at 298 K using a thermostated cell holder. Dichloromethane or CHCl₃ solution containing L was added stepwise to the CH₂Cl₂ or CHCl₃ solution of **3** (ca. 10⁻⁵ M) in a 1-cm quartz cell. The UV–visible absorption spectrum of each step was recorded by the spectrophotometer. The end point of the addition of L to the sample solution was determined by convergence of the spectral changes.

Kinetic analyses for exchange reactions in the uranyl–salophen complexes were performed by the NMR line-broadening method. Apparent first-order rate constants of exchange systems were calculated from the line width in the *slow-exchange* region for a simple two-site model^{34,35} or repetitive trial-and-error matching of theoretical spectra with the experimental spectrum measured at the appropriate temperature. In the former method, the apparent transverse relaxation time (*T*_{2obs}^{*}) of the proton in the *slow-exchange limit* was calculated from the full line width at the half-maximum ($\Delta\nu$) of its NMR spectrum and expressed in terms of the apparent natural transverse relaxation time (*T*_{2n}^{*}) and the mean lifetime of the proton in the corresponding chemical environments (τ), $T_{2obs}^*{}^{-1} = \pi\Delta\nu = T_{2n}^*{}^{-1} + \tau^{-1}$. The τ value is related to the first-order rate constant of the exchange reaction (*k*) as $\tau^{-1} = k$. The $\Delta\nu$ data of the NMR spectra were obtained by Lorentz fitting using Igor Pro 4.0.9J.³⁶ For the latter method, the computer program gNMR³⁷ was utilized to obtain the theoretical spectra at different reaction rates.

(29) Altomare, A.; Cascarano, G.; Giacovazzo, C.; Guagliardi, A. *J. Appl. Crystallogr.* **1993**, *26*, 343–350.

(30) Beurskens, P. T.; Admiraal, G.; Beurskens, G.; Bosman, W. P.; Garcia-Granda, S.; Gould, R. O.; Smits, J. M. M.; Smykalla, C. *PATY, The DIRDIF Program System*; Technical Report of the Crystallography Laboratory; University of Nijmegen: Nijmegen, The Netherlands, 1992.

(31) Beurskens, P. T.; Admiraal, G.; Beurskens, G.; Bosman, W. P.; Gelder, de R.; Israel, R.; Smits, J. M. M. *DIRDIF99: The DIRDIF99 Program System*; Technical Report of the Crystallography Laboratory; University of Nijmegen: Nijmegen, The Netherlands, 1999.

(32) Sheldrick, G. M. *SHELXL-97, Program for Crystal Structure Refinement*; University of Göttingen: Göttingen, Germany, 1997.

(33) *CrystalStructure 3.10, Crystal Structure Analysis Package*; Rigaku and Rigaku/MS: Tokyo, Japan, 2000–2002.

(34) Stengle, T. R.; Langford, C. H. *Coord. Chem. Rev.* **1967**, *2*, 349–370.

(35) Lincoln, S. F. *Prog. React. Kinetics* **1977**, *9*, 1–91.

(36) *Igor Pro*, version 4.0.9J; WaveMetrics, Inc.: Portland, OR, 2004.

(37) *gNMR*, version 5.0.4.0; Adept Scientific Inc.: Bethesda, MD, 1988–2003.

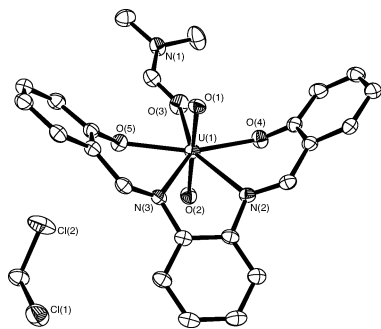


Figure 1. ORTEP view of the asymmetric unit of $\text{UO}_2(\text{salophen})\text{DMF}\cdot\text{CH}_2\text{Cl}_2$ ($1\cdot\text{CH}_2\text{Cl}_2$) at the 50% probability level.

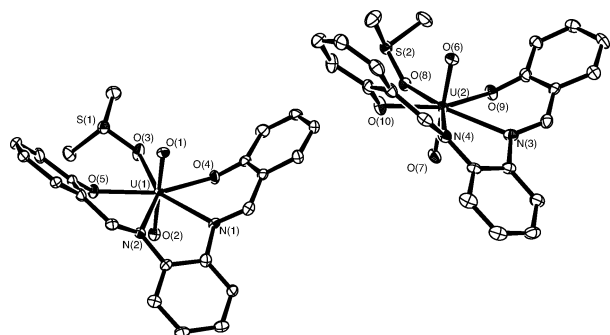


Figure 2. ORTEP view of asymmetric unit of $\text{UO}_2(\text{salophen})\text{DMSO}$ (**2**) at the 50% probability level.

3. Results and Discussion

3.1. Characterization of $\text{UO}_2(\text{salophen})\text{L}$ and $[\text{UO}_2(\text{salophen})]_2$ in the Solid State. Complexes **1** and **2** were characterized by means of single-crystal X-ray analysis. The ORTEP views of $1\cdot\text{CH}_2\text{Cl}_2$ and **2** are shown in Figures 1 and 2, respectively. Crystallographic data and selected structural parameters of these complexes are listed in Tables 1 and 2, respectively.

In Figure 1, the crystal lattice of complex **1** contains molecules of CH_2Cl_2 , which is one of the solvent components in the recrystallization. It was found that complex **1** has a pentagonal-bipyramidal geometry with an axial $\text{O}=\text{U}=\text{O}$ moiety. Generally, the salophen ligand is known to be planar in its metal complexes, because of the completely conjugated π -electron system of salophen consisting of three phenyl rings bridged by two azomethine groups.^{38–40} On the other hand, the coordinated salophen in **1** is distorted by about 35° from the equatorial plane. This is considered to be due to the bulky size of uranium. Such a distortion was also reported for $\text{UO}_2(\text{salophen})\text{EtOH}$ by Bandoli et al.³ The $\text{U}=\text{O}$ bond distances in the uranyl moiety of **1** are 1.776(2) [U(1)–O(1)] and 1.788(2) Å [U(1)–O(2)], which are typical values for uranyl compounds. The O(1)–U(1)–O(2) bond angle [$176.9(1)^\circ$] indicates that the uranyl moiety is slightly bent in the direction opposite to the coordination of DMF. The U(1)–O(4) and U(1)–O(5) bond distances [2.260(3),

2.275(3) Å] are shorter than U(1)–N(2) and U(1)–N(3) [2.549(3), 2.539(3) Å]. Such a difference might imply that the coordination of the oxygen atoms in salophen is stronger than the coordination of the nitrogen atoms. The bond distance between the oxygen atom of DMF and uranium is 2.410(3) Å [U(1)–O(3)], which is longer than those of U(1)–O(4) and U(1)–O(5). This suggests that the coordination of DMF in **1** is not as strong as the coordination of salophen.

As seen from Figure 2, complex **2** has a structure quite similar to that of **1** as follows: the pentagonal-bipyramidal geometry, the distorted salophen ligand, the typical $\text{U}=\text{O}$ bond distances in the uranyl moiety in the range of 1.78–1.79 Å, the slightly bent uranyl moiety in the direction opposite to the coordination of DMSO [$\angle\text{O}(1)–\text{U}(1)–\text{O}(2) = 176.0(2)^\circ$, $\angle\text{O}(6)–\text{U}(2)–\text{O}(7) = 176.5(2)^\circ$], and the bond distances between uranium and the coordinating atoms in salophen [U–O, 2.25–2.28 Å; U–N, 2.54–2.58 Å]. It was found that there are two molecules of **2** in the asymmetric unit of its crystal. This is caused by the different manners of coordination of DMSO to the uranium. The bond distances between the DMSO oxygen and uranium are 2.416(4) [U(1)–O(3)] and 2.408(4) Å [U(2)–O(8)], which are comparable to that in **1** [U(1)–O(3) in Figure 1 = 2.410(3) Å].

From CH_2Cl_2 or CD_2Cl_2 solutions of $\text{UO}_2(\text{salophen})\text{L}$, some red crystals precipitated. In the IR spectrum of these crystals dispersed in KBr (Figure S3), the characteristic peaks of the uranyl–salophen complexes were observed ($\nu_{\text{C}=\text{N}} = 1606\text{ cm}^{-1}$ and $\nu_3 = 920\text{ cm}^{-1}$), whereas no peaks due to **L** were detected ($\nu_{\text{C}=\text{O}}$ of DMF, $\nu_{\text{S}=\text{O}}$ of DMSO). Therefore, this compound can be concluded to be the uranyl–salophen complex without **L**.

To determine the molecular structure of the uranyl–salophen complex in the red crystal, single-crystal X-ray analysis was performed. As a result, this crystal was found to be a dimeric compound, i.e., $[\text{UO}_2(\text{salophen})]_2$ (**3**). The crystallographic data, selected structural parameters, and ORTEP views of **3** are reported in Tables 1 and 2 and Figure 3, respectively. As found for $\text{UO}_2(\text{salophen})\text{L}$, each of the $\text{UO}_2(\text{salophen})$ fragments in **3** is pentagonal-bipyramidal, and these bipyramids share the edges of the equatorial pentagons with each other. The salophen ligands in **3** are distorted in a manner similar to those in $\text{UO}_2(\text{salophen})\text{L}$ (Figures 1 and 2). This isomerizes complex **3** to the chiral pair displayed in Figure 3. Thus, this compound is racemic. The bond distances between the center uranium and the bridging oxygen atom in each $\text{UO}_2(\text{salophen})$ fragment, U(1)–O(4), U(2)–O(8), U(3)–O(11), and U(4)–O(15), are 2.39–2.40 Å, which are longer than those including the nonbridging oxygen atom, 2.20–2.23 Å [U(1)–O(3), U(2)–O(7), U(3)–O(12), and U(4)–O(16)]. Such a difference in the U–O bond distances should be caused by bridging between the $\text{UO}_2(\text{salophen})$ fragments. The bridges connecting two fragments are formed between U(1)–O(8), U(2)–O(4), U(3)–O(15), and U(4)–O(11). The lengths of these bridges are in the range from 2.46 to 2.49 Å, which are longer than those between the uranium and the oxygen atom in **L** [**1**, 2.410(3) Å; **2**, 2.416(4) and 2.408(4) Å]. There are no interactions

(38) Thornback, J. R.; Wilkinson, G. *J. Chem. Soc., Dalton Trans.* **1978**, 110–115.

(39) Suresh, E.; Bhabhade, M. M.; Srinivas, D. *Polyhedron* **1996**, *15*, 4133–4144.

(40) Zhang, K.-L.; Xu, Y.; Zheng, C.-G.; Zhang, Y.; Wang, Z.; You, X.-Z. *Inorg. Chim. Acta* **2001**, *318*, 61–66.

Table 2. Selected Structural Parameters of $\text{UO}_2(\text{salophen})\text{DMF}\cdot\text{CH}_2\text{Cl}_2$ ($1\cdot\text{CH}_2\text{Cl}_2$), $\text{UO}_2(\text{salophen})\text{DMSO}$ (**2**), and $[\text{UO}_2(\text{salophen})]_2$ (**3**)

$\text{UO}_2(\text{salophen})\text{DMF}\cdot\text{CH}_2\text{Cl}_2$ ($1\cdot\text{CH}_2\text{Cl}_2$)					
bond distances (Å)					
U(1)–O(1)	1.776(2)	U(1)–O(4)	2.260(3)	U(1)–N(2)	2.549(3)
U(1)–O(2)	1.788(2)	U(1)–O(5)	2.275(3)	U(1)–N(3)	2.539(3)
U(1)–O(3)	2.410(3)				
bond angle (deg)					
$\angle\text{O}(1)\text{--U}(1)\text{--O}(2)$	176.9(1)				
$\text{UO}_2(\text{salophen})\text{DMSO}$ (2)					
bond distances (Å)					
U(1)–O(1)	1.780(4)	U(1)–O(4)	2.255(4)	U(1)–N(1)	2.541(5)
U(1)–O(2)	1.788(5)	U(1)–O(5)	2.274(4)	U(1)–N(2)	2.545(5)
U(1)–O(3)	2.416(4)				
U(2)–O(6)	1.781(4)	U(2)–O(9)	2.270(4)	U(2)–N(3)	2.580(5)
U(2)–O(7)	1.784(5)	U(2)–O(10)	2.276(4)	U(2)–N(4)	2.551(5)
U(2)–O(8)	2.408(4)				
bond angles (deg)					
$\angle\text{O}(1)\text{--U}(1)\text{--O}(2)$	176.0(2)	$\angle\text{O}(6)\text{--U}(2)\text{--O}(7)$	176.5(2)		
$[\text{UO}_2(\text{salophen})]_2$ (3)					
bond distances (Å)					
U(1)–O(1)	1.769(7)	U(1)–O(3)	2.233(7)	U(1)–N(1)	2.540(8)
U(1)–O(2)	1.774(7)	U(1)–O(4)	2.387(6)	U(1)–N(2)	2.540(8)
U(1)–O(8)	2.463(8)				
U(2)–O(5)	1.779(7)	U(2)–O(7)	2.217(6)	U(2)–N(3)	2.546(7)
U(2)–O(6)	1.784(7)	U(2)–O(8)	2.400(6)	U(2)–N(4)	2.495(8)
U(2)–O(4)	2.475(6)				
U(3)–O(9)	1.771(7)	U(3)–O(12)	2.202(6)	U(3)–N(5)	2.560(8)
U(3)–O(10)	1.773(7)	U(3)–O(11)	2.389(7)	U(3)–N(6)	2.535(8)
U(3)–O(15)	2.491(6)				
U(4)–O(13)	1.779(7)	U(4)–O(16)	2.207(7)	U(4)–N(7)	2.512(7)
U(4)–O(14)	1.784(6)	U(4)–O(15)	2.392(7)	U(4)–N(8)	2.524(9)
U(4)–O(11)	2.445(6)				
interatomic distances (Å)					
U(1)···U(2)	3.881(1)	U(3)···U(4)	3.872(2)		
bond angles (deg)					
$\angle\text{O}(1)\text{--U}(1)\text{--O}(2)$	175.9(3)	$\angle\text{O}(5)\text{--U}(2)\text{--O}(6)$	175.5(3)		
$\angle\text{O}(9)\text{--U}(3)\text{--O}(10)$	175.4(3)	$\angle\text{O}(13)\text{--U}(4)\text{--O}(14)$	175.5(3)		

between the uranium atoms in **3** [U(1)···U(2), 3.881(1) Å; U(3)···U(4), 3.872(2) Å].

In the crystal lattice of complex **3**, a void with a volume of 328 Å³ was found. Furthermore, in the difference Fourier maps for the structure refinement of some crystals of **3**, significantly large peaks corresponding to the molecular skeleton of CH_2Cl_2 were observed in this void. On the other hand, in crystals of **3** without any solvent molecules, there

were no remarkable peaks except for ghost peaks surrounding the uranium atoms. The X-ray data of the new crystal were collected at the same temperature as those for **3**. As a result, the structure refinement of the new crystal converged on the formula $[\text{UO}_2(\text{salophen})]_2\cdot 0.5\text{CH}_2\text{Cl}_2$ (**3**·0.5 CH_2Cl_2). The crystallographic data and ORTEP view of the crystal lattice of **3**·0.5 CH_2Cl_2 are reported in Table 1 and Figure 4, respectively. The assignments of the formulas, **3** and **3**·

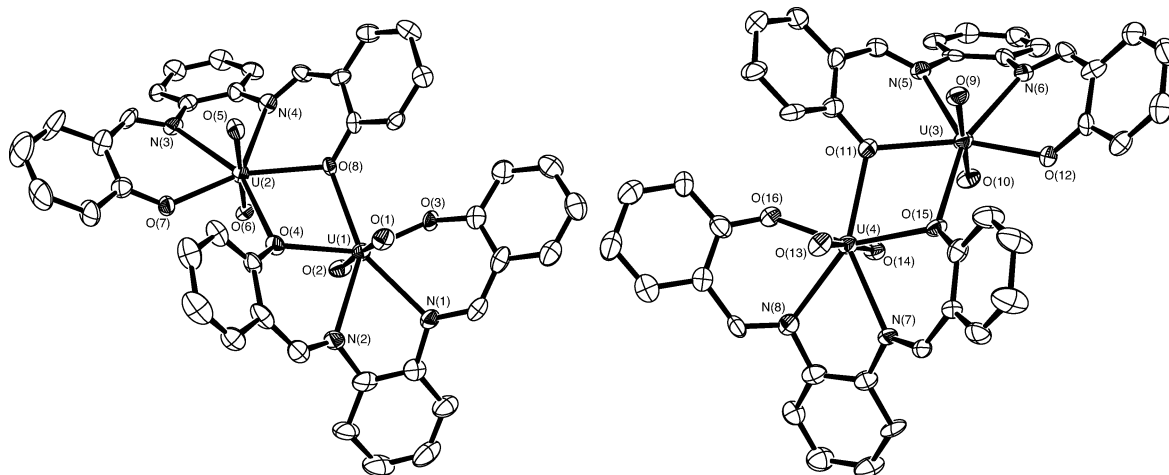


Figure 3. ORTEP views of racemic $[\text{UO}_2(\text{salophen})]_2$ (**3**) at the 50% probability level. Note that the arrangements of enantiomers of complex **3** were modified from the original crystal structure for better understanding of the structural features.

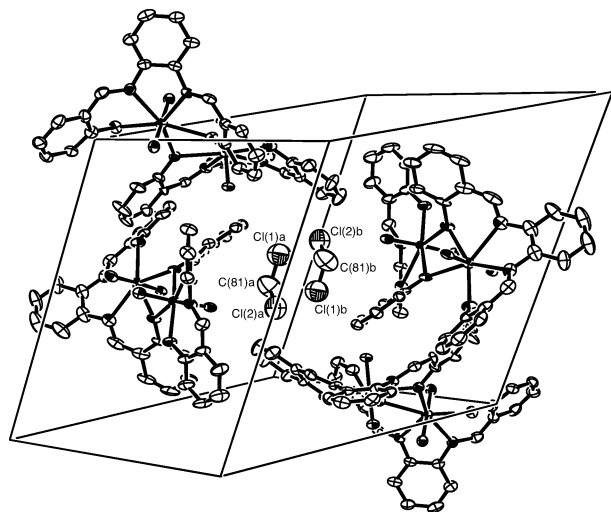


Figure 4. ORTEP view of crystal lattice of $[\text{UO}_2(\text{salophen})]_2 \cdot 0.5\text{CH}_2\text{Cl}_2$ ($3 \cdot 0.5\text{CH}_2\text{Cl}_2$).

$0.5\text{CH}_2\text{Cl}_2$, to the respective crystals are supported by the acceptable values of the agreement factors R and R_w , the goodness of fit, and the fact that the CH_2Cl_2 molecule in $3 \cdot 0.5\text{CH}_2\text{Cl}_2$ is not disordered at 93 K. The inclusion of the CH_2Cl_2 molecules and the stoichiometry of $3 \cdot 0.5\text{CH}_2\text{Cl}_2$ were also confirmed by the ^1H NMR spectrum of the CDCl_3 solution of this compound, in which the signal due to CH_2Cl_2 was observed at 5.28 ppm with a peak area indicating the composition. Surprisingly, the lattice constants and the Z value of $3 \cdot 0.5\text{CH}_2\text{Cl}_2$ are almost identical to those of **3** without the solvent molecules. Therefore, it is likely that the CH_2Cl_2 molecules are accessible to the framework consisting of **3**. Actually, the destruction of a crystal of **3** due to the rapid evaporation of the included CH_2Cl_2 molecules was confirmed by microscope observation.

3.2. $\text{UO}_2(\text{salophen})\text{L}$ in Noncoordinating Solvents. To investigate the formation of complex **3** from $\text{UO}_2(\text{salophen})\text{L}$ in noncoordinating solvents, ^1H NMR spectra of CD_2Cl_2 or CDCl_3 solutions of $\text{UO}_2(\text{salophen})\text{L}$ were measured at various temperatures.

The results for a CD_2Cl_2 solution of **1** are shown in Figure 5a. The very complicated signals in the region from 6.7 to 8.0 ppm should be assigned to the phenyl groups of salophen. At 213 K, two doublet signals due to the methyl groups of free and coordinated DMF were observed at 2.83 and 3.36 ppm, respectively. With an increase in temperature, each of the doublets first coalesced, and then the signals of free and coordinated DMF coalesced into one peak. The first coalescence can be considered to arise from a chemical exchange between the methyl groups nearer to and farther from the carbonyl oxygen in each of the free and coordinated DMF molecules, and the second one is caused by the DMF-exchange reaction between free DMF and coordinated DMF in **1**. The presence of free DMF and its exchange phenomenon were also confirmed in the signals of the formyl groups in free and coordinated DMF, which were observed at 7.92 and 9.14 ppm, respectively (213 K). It must be noted that the free DMF detected in Figure 5a results from its

dissociation from **1** and that this reaction produces the uranyl–salophen complex without DMF.

Actually, two singlet signals attributable to the azomethine group of salophen were observed at 9.39 and 9.66 ppm,¹³ which are in a lower field than that of the free H_2 salophen (8.65 ppm; see Figure S4 in the Supporting Information). Therefore, a uranyl–salophen complex different from **1** should also exist in the solution of Figure 5a. At 213 K, the peak areas of the azomethine signals (2H per salophen) at 9.39 and 9.66 ppm correspond to those of the methyl signals (6H per DMF) of the coordinated (3.36 ppm) and free (2.83 ppm) DMF in a 1:3 ratio. Therefore, these azomethine signals at 9.39 and 9.66 ppm in Figure 5a can be assigned to those in **1** and the DMF-dissociated species, respectively. With an increase in temperature from 213 to 293 K, the intensities of the azomethine signals at 9.39 and 9.66 ppm decrease and increase, respectively. Additionally, when a small amount of free DMF was added into the sample solution of Figure 5a, the azomethine signal at 9.66 ppm vanished, whereas that of **1** remained at 9.39 ppm. These results are indicative of an equilibrium between complex **1** and the DMF-dissociated species. As seen from Figure 5a, the azomethine signals at 9.39 and 9.66 ppm are separated in all temperature ranges despite the exchange phenomenon of DMF in **1**. Hence, the equilibrium between complex **1** and the DMF-dissociated species seems to be independent of the DMF-exchange reaction in **1**. Thus, the possibility of a monomeric $\text{UO}_2(\text{salophen})$ complex as the DMF-dissociated species can be excluded, because $\text{UO}_2(\text{salophen})$ is also an intermediate of the DMF-exchange reaction in **1**. It is straightforward that the DMF-dissociated species observed in Figure 5a is assigned to complex **3**, because this dimeric compound was actually obtained from the CH_2Cl_2 solution of $\text{UO}_2(\text{salophen})\text{L}$.

The ^1H NMR spectra of the CD_2Cl_2 solution of **2** were also measured at various temperatures and are displayed in Figure 5b. As a result, similar phenomena were observed. At 213 K, signals corresponding to free and coordinated DMSO were observed at 2.54 and 3.14 ppm, respectively. With an increase in temperature, these signals broadened and finally coalesced into one peak, indicating the DMSO-exchange reaction in **2**. Azomethine signals assumed to be due to **2** and **3** were detected at 9.38 and 9.67 ppm, respectively. These assignments for the azomethine signals (2H) were established by the consistency in the ratios of the peak areas relative to those of free and coordinated DMSO (6H) at 213 K. As the temperature was increased, the peak intensities of the azomethine signals at 9.38 and 9.67 ppm decreased and increased, respectively. This implies an equilibrium between **2** and **3**.

Similar NMR results were obtained in CDCl_3 solutions of **1** and **2** (see Figure S5). At 213 K, the NMR signals of the methyl and formyl groups of DMF were observed at 2.93 and 8.01 ppm, respectively, for the free ligand and at 3.39 and 9.20 ppm, respectively, for the coordinated ligand (Figure S5a). The azomethine signals attributable to **1** and **3** appeared at 9.35 and 9.55 ppm (213 K), respectively. For $\text{L} = \text{DMSO}$ (Figure S5b), the methyl signals of free and coordinated

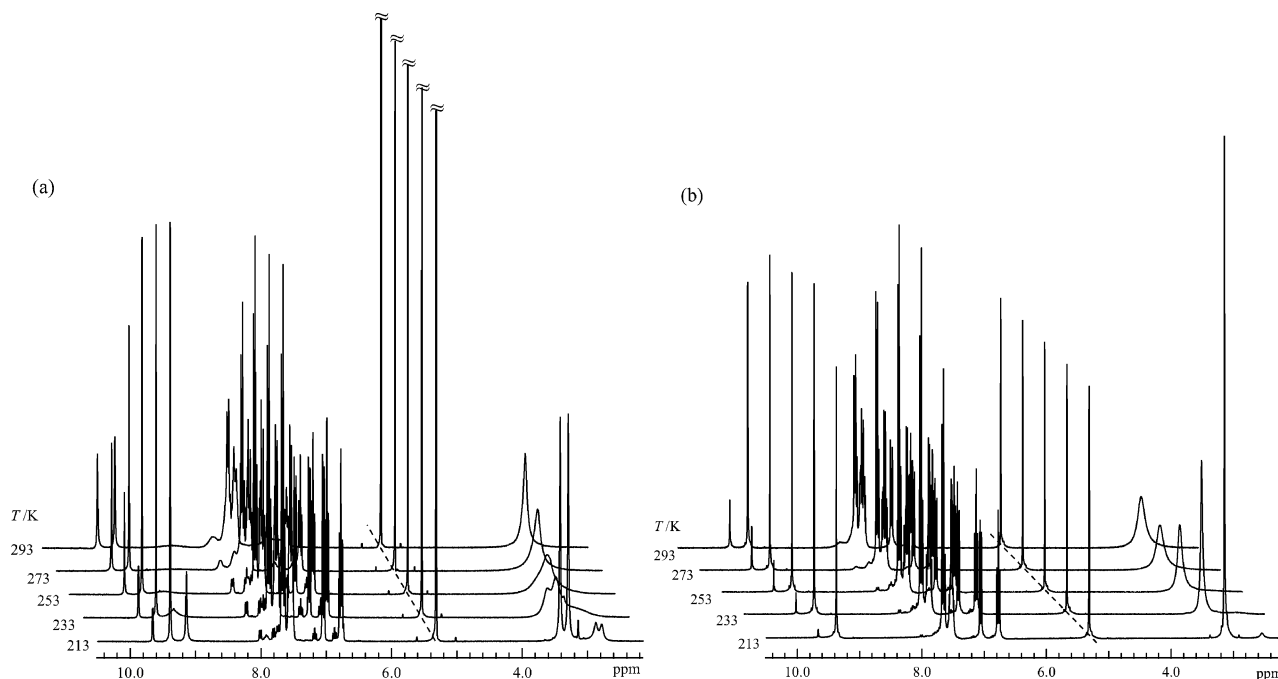


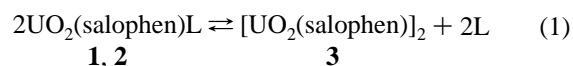
Figure 5. ^1H NMR spectra of CD_2Cl_2 solutions of (a) $\text{UO}_2(\text{salophen})\text{DMF}$ (**1**, 1.29×10^{-2} M) and (b) $\text{UO}_2(\text{salophen})\text{DMSO}$ (**2**, 1.57×10^{-2} M) measured at various temperatures. A small peak at 3.15 ppm in part a is due to the impurity of the solvent.

DMSO were detected at 2.68 and 3.20 ppm (223 K), respectively. The azomethine signals of **2** and **3** were observed at 9.37 and 9.59 ppm (223 K), respectively. From a comparison between the results in CD_2Cl_2 and CDCl_3 solutions, it seems that complex **3** is produced more readily in CDCl_3 than in CD_2Cl_2 .

Interestingly, in the ^1H NMR spectra of CDCl_3 solutions of $\text{UO}_2(\text{salophen})\text{L}$ (Figure S5), the singlet azomethine signal of **3** observed at 296 K was split into two peaks with a decrease in temperature. This indicates that there are two different sites of the azomethine groups in **3** and that these are chemically exchangeable with each other. Actually, complex **3** has two chemical environments for the azomethine groups nearer to and farther from the bridging phenoxides, as shown in Figure 3. Furthermore, these azomethine groups are exchangeable with each other by the exchange reaction between the enantiomers of **3**. In the CD_2Cl_2 systems (Figure 5), the splitting of the azomethine signal of **3** was not observed despite all of the other data indicating the formation of **3**. This overlap of the azomethine signals in the different sites might be expected from the magnetic anisotropy of the uranyl ion or solvent effect. In previous articles,^{41,42} the degeneration of two signals arising from the methyl groups of coordinated DMF in $\text{UO}_2(\text{DMF})_5^{2+}$ was observed and explained by the effect of the magnetic anisotropy around the metal ion.⁴³ On the other hand, two azomethine signals of **3** can be observed separately in the CDCl_3 solution at lower temperature. Additionally, the chemical shift values of the azomethine

signals of **3** in CD_2Cl_2 solution differ from those in CDCl_3 by ca. 0.1 ppm.⁴⁴ These results indicate that the chemical shifts of the azomethine signals of **3** are surely affected by the solvent. Thus, the overlap of the azomethine signals of **3** in the CD_2Cl_2 solution might be caused by the effect of the solvent rather than by the effect of magnetic anisotropy.

3.3. Equilibrium between $\text{UO}_2(\text{salophen})\text{L}$ and $[\text{UO}_2(\text{salophen})]_2$. For the formation of complex **3** from $\text{UO}_2(\text{salophen})\text{L}$ (L = DMF, DMSO) in CH_2Cl_2 and CHCl_3 , the following dimerization equilibrium can be proposed



$$K_{\text{dim}} = \frac{[[\text{UO}_2(\text{salophen})]_2][\text{L}]^2}{[\text{UO}_2(\text{salophen})\text{L}]^2} \quad (2)$$

where K_{dim} is the equilibrium constant of eq 1.

To confirm the validity of eq 1, the dependence of the UV–visible absorption spectrum on the concentration of L was examined for CH_2Cl_2 and CHCl_3 solutions of **3** at 298 K. The spectral changes in the system with L = DMF and solvent = CH_2Cl_2 are shown in Figure 6. In these UV–visible absorption spectra, isosbestic points are clearly observed. This indicates that only one equilibrium is present. Similar phenomena were observed in other combinations of L and solvent, as shown in Figures S6–S8 in the Supporting Information.

(41) Bowen, R. P.; Honan, G. J.; Lincoln, S. F.; Spotswood, T. M.; Williams, E. H. *Inorg. Chim. Acta* **1979**, *33*, 235–239.

(42) Doine, H.; Ikeda, Y.; Tomiyasu, H.; Fukutomi, H. *Bull. Chem. Soc. Jpn.* **1983**, *56*, 1989–1994.

(43) Pople, J. A.; Schneider, W. G.; Bernstein, H. J. *High-Resolution Nuclear Magnetic Resonance*; McGraw-Hill: New York, 1959.

(44) To exclude an effect of any trace of acid in the solvent, CDCl_3 was treated on alumina, and then the ^1H NMR spectra of the CDCl_3 solution of complex **3** were measured again at 293 and 213 K. As a result, no differences were observed in the azomethine signals of complex **3** in Figures S5 and 11b.

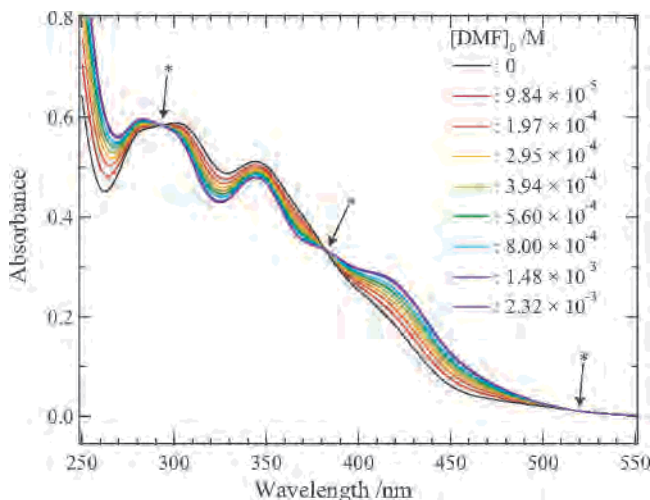


Figure 6. Dependence of UV–visible absorption spectra on the concentration of DMF at 298 K. $[[\text{UO}_2(\text{salophen})]_2]_0 = 1.26 \times 10^{-5}$ M, CH_2Cl_2 system. Asterisks indicate the isosbestic points.

According to eq 1, the absorbance (A) observed in the UV–visible absorption spectra is given by

$$A = \epsilon_{\text{mono}}[\text{UO}_2(\text{salophen})\text{L}] + \epsilon_{\text{dim}}[[\text{UO}_2(\text{salophen})]_2] \quad (3)$$

where ϵ_{mono} and ϵ_{dim} are molar absorptivities of $\text{UO}_2(\text{salophen})\text{L}$ and **3**, respectively. These values are calculated by eqs 4 and 5, respectively

$$\epsilon_{\text{mono}} = \frac{A_{\text{mono}}}{2[[\text{UO}_2(\text{salophen})]_2]_0} \quad (4)$$

$$\epsilon_{\text{dim}} = \frac{A_{\text{dim}}}{[[\text{UO}_2(\text{salophen})]_2]_0} \quad (5)$$

where A_{mono} , A_{dim} , and $[[\text{UO}_2(\text{salophen})]_2]_0$ are the absorbance of $\text{UO}_2(\text{salophen})\text{L}$ at the convergence of the spectral change with the addition of L, the absorbance of **3** prior to the addition of L, and the initial concentration of **3** dissolved in each sample solution, respectively.

The mass balances of the $\text{UO}_2(\text{salophen})$ unit and L in the sample solution are given as

$$2[[\text{UO}_2(\text{salophen})]_2]_0 = [\text{UO}_2(\text{salophen})\text{L}] + 2[[\text{UO}_2(\text{salophen})]_2] \quad (6)$$

$$[\text{L}]_0 = [\text{UO}_2(\text{salophen})\text{L}] + [\text{L}] \quad (7)$$

The total concentration of L is denoted by $[\text{L}]_0$.

By using eqs 2–7, the absorbance A observed in Figures 6 and S6–S8 can be expressed as a function of $[\text{L}]_0/[\text{L}]$, that is

$$A = K_{\text{dim}}(\epsilon_{\text{dim}} - 2\epsilon_{\text{mono}}) \left(\frac{[\text{L}]_0}{[\text{L}]} - 1 \right)^2 + 2\epsilon_{\text{mono}}[[\text{UO}_2(\text{salophen})]_2]_0 \quad (8)$$

The values of $[\text{L}]_0/[\text{L}]$ were calculated using eqs 9 and 10

$$\frac{[\text{L}]_0}{[\text{L}]} = \frac{[\text{L}]_0}{[\text{L}]_0 - [\text{UO}_2(\text{salophen})\text{L}]} \quad (9)$$

$$[[\text{UO}_2(\text{salophen})]_2] = 2[[\text{UO}_2(\text{salophen})]_2]_0 \frac{|A - A_{\text{dim}}|}{|A_{\text{mono}} - A_{\text{dim}}|} \quad (10)$$

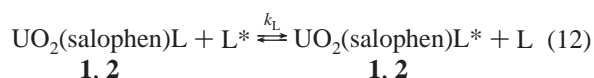
The absorbancies at 430 nm in Figures 6 and S6–S8 were plotted against $[\text{L}]_0/[\text{L}]$ as shown in Figure 7. To estimate K_{dim} at 298 K, the least-squares fit of eq 8 to the experimental points was performed for each system. The parameters obtained by the best fit are summarized in Table 3. As seen from Figure 7, the best-fit curves of eq 8 well reproduce the experimental points. The calculated values of K_{dim} at 298 K and their logarithms are also listed in the two rightmost columns of Table 3. Consequently, it was demonstrated spectrophotometrically that complex **3** remains its dimeric structure even in CH_2Cl_2 and CHCl_3 solutions. Therefore, the ^1H NMR signals observed at 9.66 or 9.67 ppm in CD_2Cl_2 (Figure 5) and 9.55 or 9.59 ppm in CDCl_3 (Figure S5) are concluded to be due to the azomethine groups of **3**.

It was feasible to estimate the thermodynamic parameters of eq 1 from the temperature dependence of K_{dim} calculated by the peak areas of the azomethine signals in Figures 5 and S5. The resulting semilogarithmic plots of K_{dim} vs reciprocal temperature are shown in Figure 8. By using the relationship

$$K_{\text{dim}} = \exp \left[-\frac{\Delta H_{\text{dim}}}{R} \cdot \frac{1}{T} + \frac{\Delta S_{\text{dim}}}{R} \right] \quad (11)$$

where ΔH_{dim} , ΔS_{dim} , and R are the formation enthalpy and entropy of eq 1 and the gas constant, respectively, the thermodynamic parameters of eq 1 in each system were evaluated. The formation free energy at 298 K ($\Delta G_{\text{dim}}^{298}$) for each system was calculated as $\Delta G_{\text{dim}} = \Delta H_{\text{dim}} - T\Delta S_{\text{dim}}$. The values obtained for ΔH_{dim} , ΔS_{dim} , $\Delta G_{\text{dim}}^{298}$, and $\log K_{\text{dim}}$ at 298 K are summarized in Table 4. In both cases of L = DMF and DMSO, the $\Delta G_{\text{dim}}^{298}$ values for the CDCl_3 systems are smaller than those for the CD_2Cl_2 system by 5–6 $\text{kJ}\cdot\text{mol}^{-1}$. This suggests that the formation of **3** is favored more in CDCl_3 than CD_2Cl_2 . Furthermore, the $\Delta G_{\text{dim}}^{298}$ values indicate that complex **3** is generated more readily from **1** than from **2** in each solvent. This is suggestive of the difference in the coordination ability of L to the $\text{UO}_2(\text{salophen})$ unit ($\text{DMF} < \text{DMSO}$). It should be emphasized that each of the $\log K_{\text{dim}}$ values at 298 K estimated from the ^1H NMR data is comparable to that determined by the UV–visible absorption spectral changes shown in Table 3.

3.4. Exchange Reactions of L in $\text{UO}_2(\text{salophen})\text{L}$. To obtain information concerning the reaction mechanism of the dimerization equilibrium between $\text{UO}_2(\text{salophen})\text{L}$ and **3** (eq 1), the kinetics of the L-exchange reactions in (eq 12) was studied



where k_L is the apparent first-order rate constant and the asterisk is a typographical distinction only.

The ^1H NMR spectra of CD_2Cl_2 solutions containing $\text{UO}_2(\text{salophen})\text{L}$ and free L were measured at various tempera-

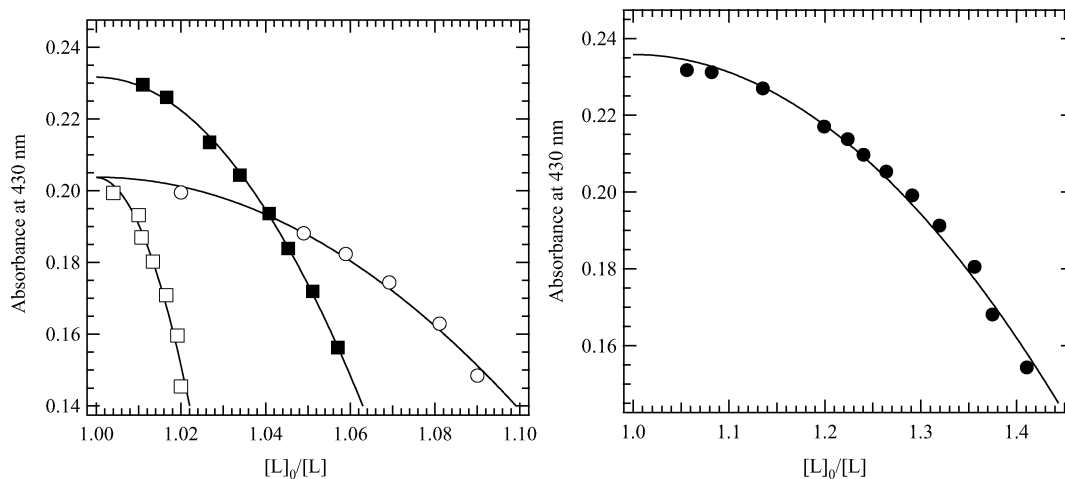


Figure 7. Plots of absorbancies at 430 nm in Figures 6 and S6–S8 vs $[L]_0/[L]$. Solid squares, L = DMF, CH_2Cl_2 system (Figure 6); solid circles, L = DMSO, CH_2Cl_2 system (Figure S6); open squares, L = DMF, CHCl_3 system (Figure S7); open circles, L = DMSO, CHCl_3 system (Figure S8). Smooth curves are the best fits of eq 8 to the experimental data.

Table 3. Parameters in the Best Fits of eq 8 to Absorbance Changes at 430 nm in Figures 6 and S6–S8 at 298 K

L	solvent	ϵ_{dim}^a ($\text{M}^{-1}\cdot\text{cm}^{-1}$)	ϵ_{mono}^b ($\text{M}^{-1}\cdot\text{cm}^{-1}$)	$[\text{UO}_2(\text{salophen})]_2$ (M)	K_{dim}^{298} (M)	$\log K_{\text{dim}}^{298}$
DMF	CH_2Cl_2	1.08×10^4	9.2×10^3	1.26×10^{-5}	$(3.1 \pm 0.1) \times 10^{-3}$	-2.51 ± 0.01
DMF	CHCl_3	1.08×10^4	8.6×10^3	1.19×10^{-5}	$(2.1 \pm 0.1) \times 10^{-2}$	-1.68 ± 0.02
DMSO	CH_2Cl_2	1.09×10^4	9.4×10^3	1.26×10^{-5}	$(5.9 \pm 0.1) \times 10^{-5}$	-4.23 ± 0.01
DMSO	CHCl_3	1.08×10^4	8.9×10^3	1.15×10^{-5}	$(9.4 \pm 0.3) \times 10^{-4}$	-3.03 ± 0.02

^a Calculated using eq 5 and fixed in the least-squares fit process. ^b Result in the least-squares fit, which agrees with the ϵ_{mono} values evaluated from the experimental absorption spectra and eq 4 within 1–2% error for each system. ^c Equilibrium constant of eq 1 at 298 K.

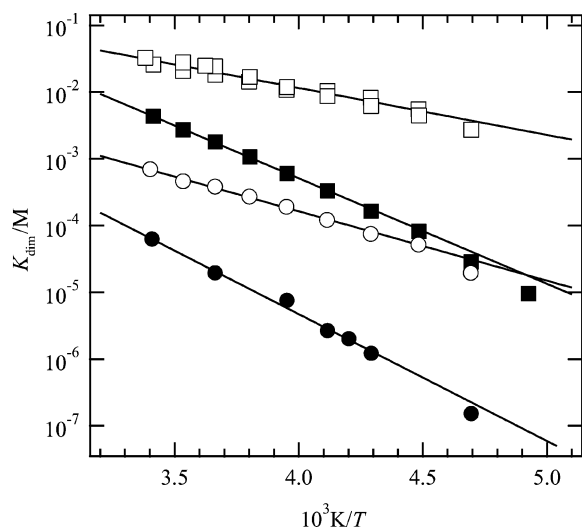


Figure 8. Semilogarithmic plots of K_{dim} in eq 1 calculated from peak areas in ^1H NMR spectra (Figures 5 and S5) vs reciprocal temperature. Solid squares, L = DMF, CD_2Cl_2 system; open squares, L = DMF, CDCl_3 system; solid circles, L = DMSO, CD_2Cl_2 system; open circles, L = DMSO, CDCl_3 system.

tures. The concentrations of $\text{UO}_2(\text{salophen})\text{L}$ and free L were selected from the K_{dim} data to prevent the formation of **3** in each sample. In the resulting ^1H NMR spectra, the signals due to free and coordinated L were detected separately at 203 and 213 K and broadened and finally coalesced into one peak with an increase in temperature as observed in Figures 5 and S5. The kinetic analyses of the L-exchange reactions were performed with the simple two-site model using the singlet ^1H signals of the formyl group of DMF for

Table 4. Thermodynamic Parameters of eq 1 Derived from ^1H NMR Spectra

L	solvent	ΔH_{dim}^a	ΔS_{dim}^b	$\Delta G_{\text{dim}}^{298}$ ^c	$\log K_{\text{dim}}^{298}$ ^d
DMF	CD_2Cl_2	30 ± 1	58 ± 1	13 ± 1	-2.3 ± 0.1
DMF	CDCl_3	13 ± 1	17 ± 4	8 ± 2	-1.5 ± 0.4
DMSO	CD_2Cl_2	36 ± 1	44 ± 4	23 ± 2	-4.1 ± 0.4
DMSO	CDCl_3	20 ± 1	7 ± 3	18 ± 2	-3.1 ± 0.3

^a Formation enthalpy in $\text{kJ}\cdot\text{mol}^{-1}$. ^b Formation entropy in $\text{J}\cdot\text{mol}^{-1}\cdot\text{K}^{-1}$. ^c Formation free energy at 298 K in $\text{kJ}\cdot\text{mol}^{-1}$. ^d Equilibrium constant of eq 1 at 298 K.

1 and the methyl group of DMSO for **2**. The k_L values obtained by the spectrum simulation were plotted against reciprocal temperature as shown in Figure 9.

In Figure 9, the k_{DMF} value at each temperature is found to increase with increasing concentration of free DMF ($[\text{DMF}]_{\text{free}}$). Figure 10 shows plots of k_{DMF} against $[\text{DMF}]_{\text{free}}$. As seen from this figure, the k_{DMF} value at each temperature depends linearly on $[\text{DMF}]_{\text{free}}$ with an intercept. Thus, the k_{DMF} value should be expressed as

$$k_{\text{DMF}} = k_1 + k_2[\text{DMF}]_{\text{free}} \quad (13)$$

This suggests that the DMF-exchange reaction in **1** proceeds through two pathways independent of and dependent on $[\text{DMF}]_{\text{free}}$. The k_1 path should be categorized as a *dissociative* mechanism.⁴⁵ For the mechanism of k_2 path, there are two candidates, i.e., *interchange* and *associative* mechanisms.⁴⁵ In the former mechanism, k_{DMF} can be expressed as

(45) Helm, L.; Merbach, A. E. *Chem. Rev.* **2005**, *105*, 1923–1959.

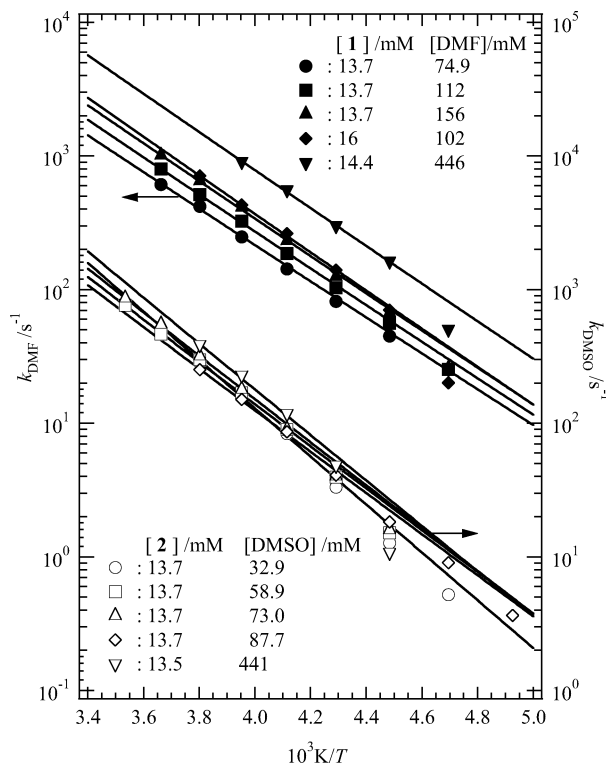


Figure 9. Temperature dependence of k_1 . Solid symbols, L = DMF [$\text{UO}_2(\text{salophen})\text{DMF}$, **1**], open symbols, L = DMSO [$\text{UO}_2(\text{salophen})\text{DMSO}$, **2**]. The smooth line for each plot is the best fit of the Eyring relationship (eq 15) to the experimental results.

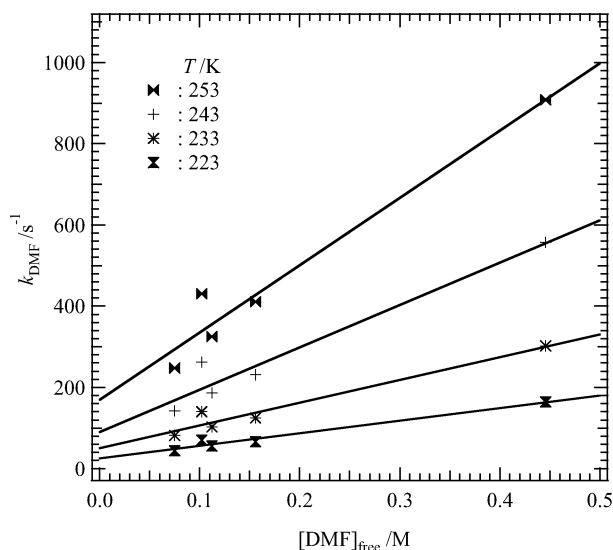


Figure 10. $[\text{DMF}]_{\text{free}}$ dependence of k_{DMF} for the DMF-exchange reaction in $\text{UO}_2(\text{salophen})\text{DMF}$ (**1**) in CD_2Cl_2 .

$$k_{\text{DMF}} = \frac{k_1 + k_i K_{\text{OS}} [\text{DMF}]_{\text{free}}}{1 + K_{\text{OS}} [\text{DMF}]_{\text{free}}} \quad (14)$$

where k_i and K_{OS} are the first-order rate constant for the interchange path and the formation constant of an outer-sphere complex such as $\mathbf{1} \cdots \text{DMF}$, respectively. To explain the linear relationship of k_{DMF} on $[\text{DMF}]_{\text{free}}$ in Figure 10, the value of $K_{\text{OS}}[\text{DMF}]_{\text{free}}$ in eq 14 must be much smaller than unity, even under high- $[\text{DMF}]_{\text{free}}$ conditions, i.e., $K_{\text{OS}} < 10^{-1} \text{ M}^{-1}$. From this upper limit of K_{OS} , the lower limits of k_i at 223, 233, 243, and 253 K can be derived as (0.31,

$0.56, 1.0,$ and $1.8) \times 10^4 \text{ s}^{-1}$, respectively. However, it seems that these lower limits of k_i are too large in comparison with the corresponding value for the DMSO-exchange reaction in $\text{UO}_2(\text{acac})_2$ DMSO ($k_i = 57 \text{ s}^{-1}$, $K_{\text{OS}} = 6.2 \text{ M}^{-1}$ at 253 K).⁴⁶ The alternative mechanism for k_2 , the associative pathway, should be more plausible for k_2 , because k_{DMF} can be written simply by eq 13. If free DMF approaches complex **1** from the opposite direction of the phenoxide groups distorted from the equatorial plane to avoid the steric hindrance, this mechanism might be possible. Therefore, in the $[\text{DMF}]_{\text{free}}$ region examined here, the DMF-exchange mechanisms for k_1 and k_2 in eq 13 are assigned to the dissociative and associative pathways, respectively.

The k_1 and k_2 values at each temperature were evaluated from the intercepts and slopes, respectively, of the best-fit lines in Figure 10 and plotted against the reciprocal temperature in Figure S11. The activation parameters were estimated by the least-squares fit of the Eyring equation (eq 15) to the experimental results in Figure S11

$$k_L = \frac{k_B T}{h} \exp\left(-\frac{\Delta H_L^\ddagger}{R} \frac{1}{T} + \frac{\Delta S_L^\ddagger}{R}\right) \quad (15)$$

where k_B , h , ΔH_L^\ddagger , and ΔS_L^\ddagger are the Boltzmann constant, the Planck constant, and the activation enthalpy and entropy of the L-exchange reactions in $\text{UO}_2(\text{salophen})\text{L}$, respectively.⁴⁷ The resulting values were $\Delta H_1^\ddagger = 28 \pm 1 \text{ kJ}\cdot\text{mol}^{-1}$ and $\Delta S_1^\ddagger = -89 \pm 4 \text{ J}\cdot\text{mol}^{-1}\cdot\text{K}^{-1}$ for k_1 and $\Delta H_2^\ddagger = 24 \pm 1 \text{ kJ}\cdot\text{mol}^{-1}$ and $\Delta S_2^\ddagger = -88 \pm 4 \text{ J}\cdot\text{mol}^{-1}\cdot\text{K}^{-1}$ for k_2 . By using these parameters, the k_1 and k_2 values at 298 K were calculated as $(1.5 \pm 0.1) \times 10^3 \text{ s}^{-1}$ and $(1.1 \pm 0.1) \times 10^4 \text{ M}^{-1}\cdot\text{s}^{-1}$, respectively.

On the other hand, there is no significant dependence of k_{DMSO} on $[\text{DMSO}]_{\text{free}}$ in Figure 9. This suggests that the DMSO-exchange reaction in **2** occurs dissociatively. From eq 15, the activation parameters and k_{DMSO} at 298 K were evaluated as $\Delta H_{\text{DMSO}}^\ddagger = 30 \pm 1 \text{ kJ}\cdot\text{mol}^{-1}$, $\Delta S_{\text{DMSO}}^\ddagger = -84 \pm 4 \text{ J}\cdot\text{mol}^{-1}\cdot\text{K}^{-1}$, and $k_{\text{DMSO}} = (1.7 \pm 0.1) \times 10^3 \text{ s}^{-1}$. The slightly larger value of $\Delta H_{\text{DMSO}}^\ddagger$ compared to the corresponding value for L = DMF (ΔH_1^\ddagger) might be caused by the stronger coordination of DMSO to the $\text{UO}_2(\text{salophen})$ unit than DMF.

To generate complex **3** from $\text{UO}_2(\text{salophen})\text{L}$, the coordinated L in $\text{UO}_2(\text{salophen})\text{L}$ must be dissociated in the process of eq 1. There are two possibilities for the reaction process from $\text{UO}_2(\text{salophen})\text{L}$ to **3**, i.e., the L dissociation from the $\text{UO}_2(\text{salophen})$ unit can occur *before* or *after* the formation of a dimer. However, the latter path is unlikely, because the predictable intermediate or activation complex $[\text{UO}_2(\text{salophen})\text{L}]_2$ is sterically unfavorable. Hence, eq 1 might proceed via the intermediate $\text{UO}_2(\text{salophen})$. The same discussion is also applicable to the back reaction of eq 1. For the formation of $\text{UO}_2(\text{salophen})\text{L}$ from complex **3** and

(46) Ikeda, Y.; Tomiyasu, H.; Fukutomi, H. *Bull. Chem. Soc. Jpn.* **1983**, *56*, 1060–1066.

(47) The subscript L of ΔH^\ddagger , ΔS^\ddagger , and k in eq 15 was replaced by the appropriate subscripts for k_1 , k_2 , and k_{eex} , i.e., 1, 2, and eex, respectively.

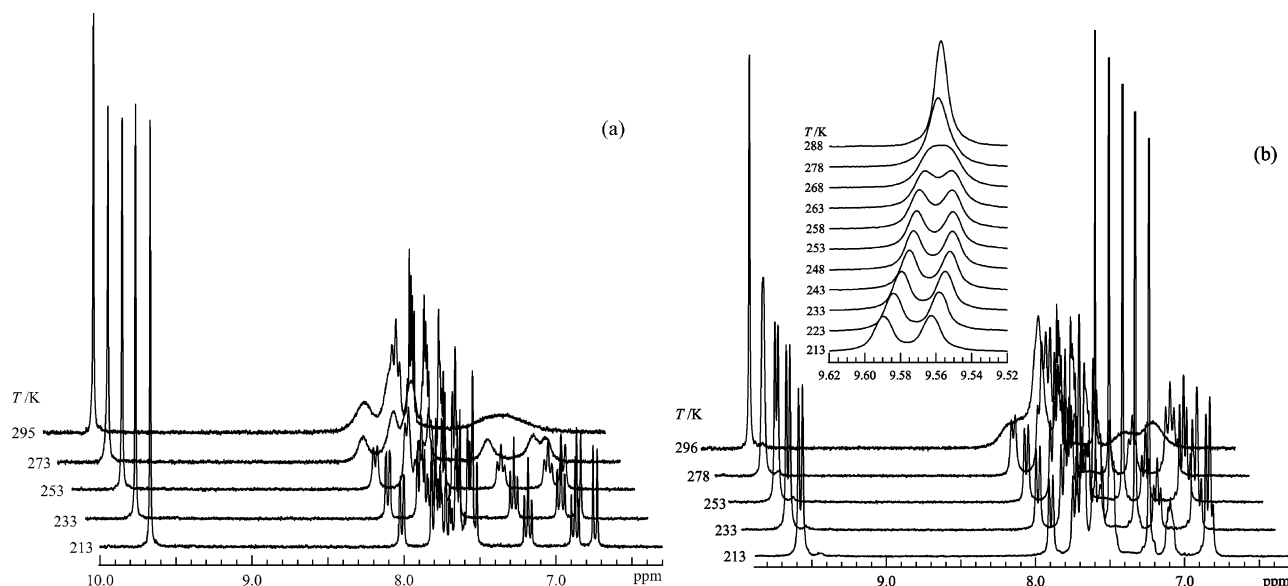
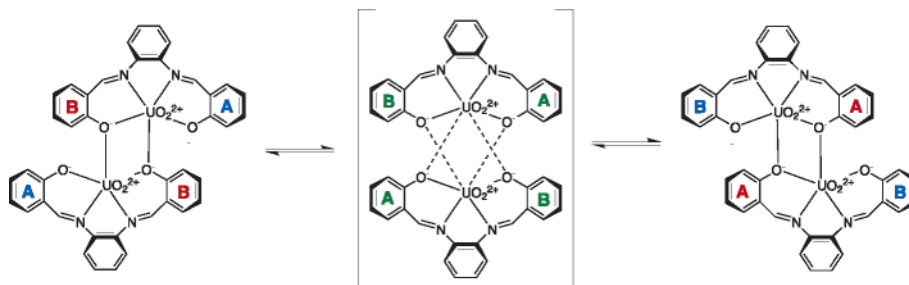


Figure 11. ^1H NMR spectra of (a) CD_2Cl_2 and (b) CDCl_3 solutions of $[\text{UO}_2(\text{salophen})]_2$ (**3**). Inset in part b: Temperature dependence of the azomethine signals magnified in the range from 9.52 to 9.62 ppm.

Scheme 1. Sliding Model for the Enantiomer Exchange of $[\text{UO}_2(\text{salophen})]_2$ (**3**)^a



^a Red, blue, and green colors of the letters A and B indicate the bridging and nonbridging phenoxide groups and that in the intermediate, respectively.

free L, it should be necessary to pass through the dissociation of the $\text{UO}_2(\text{salophen})$ fragments in **3**, followed by the coordination of L to the intermediate $\text{UO}_2(\text{salophen})$. It must be noted that this intermediate is common to that in the dissociative path of eq 12. Nevertheless, as pointed out from Figures 5 and S5, eq 1 seems to be independent of eq 12. This suggests that eq 1 proceeds via an additional rate-determining step. The additional step might be controlled by the encounter between the $\text{UO}_2(\text{salophen})$ intermediates, because this intermediate should be a short-lived species and, therefore, its concentration in solution must be very small.

3.5. ^1H NMR Spectrum of $[\text{UO}_2(\text{salophen})]_2$. The ^1H NMR spectra of CD_2Cl_2 and CDCl_3 solutions of complex **3** were measured at various temperatures. The results are shown in Figure 11.

In CD_2Cl_2 (Figure 11a), the singlet signal assigned to the azomethine group in **3** was observed at 9.67 ppm, which is consistent with the signal at 9.66 or 9.67 ppm in Figure 5. Moreover, the phenyl signals in the range from 6.7 to 8.0 ppm were found to be well-resolved at 213 K and to be broadened and finally coalesced with increasing temperature. This phenomenon is suggestive of an intramolecular exchange reaction between the enantiomers of **3**. Dalla Cort et al. proposed that the monomeric $\text{UO}_2(\text{salophen})$ and its

derivatives without L in the fifth equatorial site, the molecular structures of which have not been sufficiently identified, show intramolecular exchange reactions through a flipping motion of the distorted salophen ligand.^{48–50} However, if such a flipping model is also applicable to the enantiomer exchange of **3**, the bridging and nonbridging phenoxide groups in **3** should not exchange with each other as shown in Scheme S1 in Supporting Information. This means that no exchange aspects of the phenyl groups in **3** should be observed in the ^1H NMR spectra. Therefore, the flipping model can be ruled out for the exchange phenomenon observed in Figure 11a. Another candidate for the reaction mechanism of the enantiomer exchange is the sliding model shown in Scheme 1. In this model, the bridging and nonbridging phenoxide groups can exchange with each other. If the $\text{UO}_2(\text{salophen})$ fragments are completely separated in the process of the enantiomer exchange of **3**, the intermediate $\text{UO}_2(\text{salophen})$ unit can form $\text{UO}_2(\text{salophen})\text{L}$ with free L or return to **3**. In this case, the enantiomer exchange of **3** is

(48) Dalla Cort, A.; Mandolini, L.; Palmieri, G.; Pasquini, C.; Schiaffino, L. *Chem. Commun.* **2003**, 2178–2179.

(49) Dalla Cort, A.; Gasparrini, F.; Lunazzi, L.; Mandolini, L.; Mazzanti, A.; Pasquini, C.; Pierini, M.; Rompietti, R.; Schiaffino, L. *J. Org. Chem.* **2005**, *70*, 8877–8883.

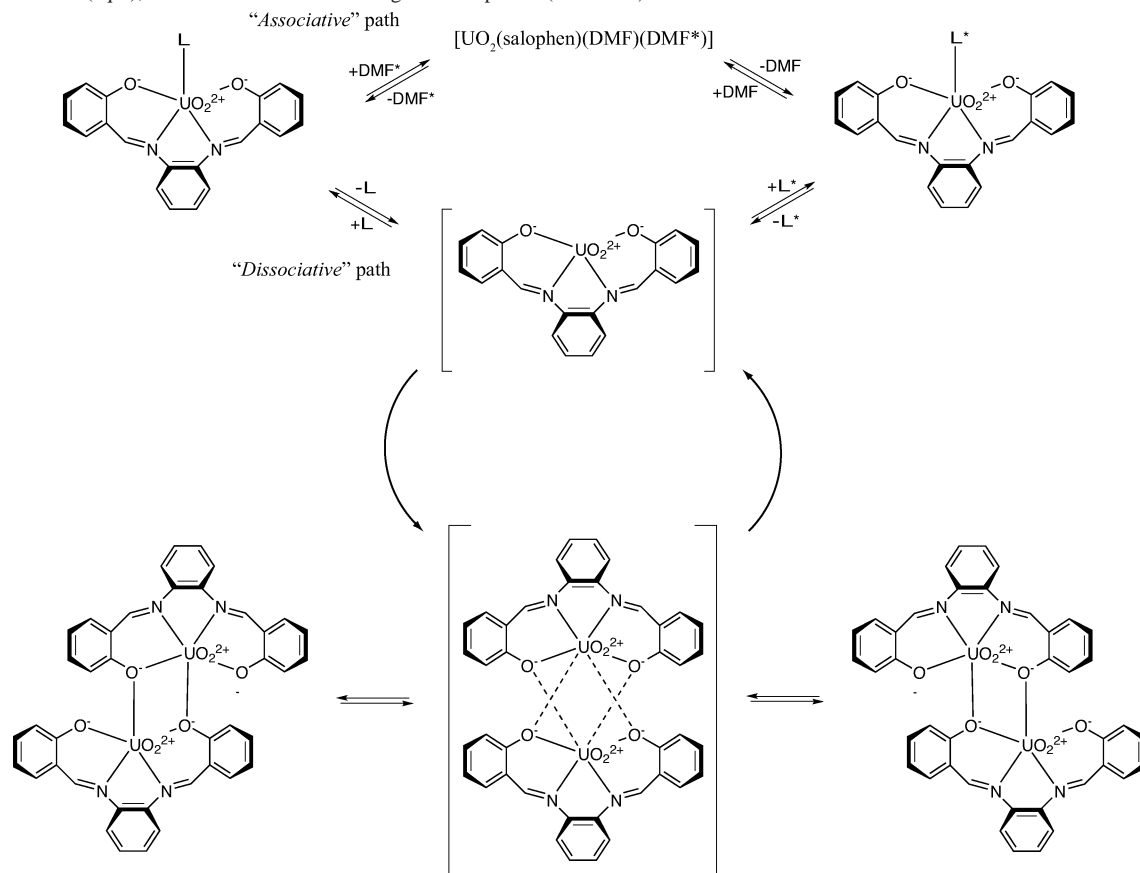
(50) Dalla Cort, A.; Mandolini, L.; Pasquini, C.; Schiaffino, L. *J. Org. Chem.* **2005**, *70*, 9814–9821.

Table 5. Summary of Thermodynamic and Kinetic Data for the Reactivity of Uranyl–Salophen Complexes

complex	L	solvent	dimerization equilibrium				ligand exchange/enantiomer exchange			
			$\Delta H_{\text{dim}}^{a,b}$	$\Delta S_{\text{dim}}^{a,c}$	$\Delta G_{\text{dim}}^{298 a,b}$	$\log K_{\text{dim}}^{298 a}$	$\Delta H^{\ddagger b}$	$\Delta S^{\ddagger c}$	$k^{298 d}$	mechanism
$\text{UO}_2(\text{salophen})\text{L}$	DMF	CH_2Cl_2	30 ± 1	58 ± 1	13 ± 1	-2.51 ± 0.01	28 ± 1^e	-89 ± 4^e	$(1.5 \pm 0.1) \times 10^3$	D^g
		CHCl_3	13 ± 1	17 ± 4	8 ± 2	-1.68 ± 0.02	—	—	—	—
		DMSO	36 ± 1	44 ± 4	23 ± 2	-4.23 ± 0.01	30 ± 1^e	-84 ± 4^e	$(1.7 \pm 0.1) \times 10^3$	D^g
		CHCl_3	20 ± 1	7 ± 3	18 ± 2	-3.03 ± 0.02	—	—	—	—
$[\text{UO}_2(\text{salophen})]_2$	—	CHCl_3	—	—	—	—	61 ± 6^i	-3 ± 24^i	87	sliding ^j

^a Thermodynamic parameters in dimerization equilibrium eq 1. ^b In $\text{kJ}\cdot\text{mol}^{-1}$. ^c In $\text{J}\cdot\text{mol}^{-1}\cdot\text{K}^{-1}$. ^d First-order rate constant at 298 K in s^{-1} . ^e Activation parameters of L-exchange reaction in $\text{UO}_2(\text{salophen})\text{L}$ (**1**, **2**). ^f Second-order rate constant at 298 K in $\text{M}^{-1}\cdot\text{s}^{-1}$. ^g Dissociative mechanism. ^h Associative mechanism. ⁱ Activation parameters in enantiomer exchange of $[\text{UO}_2(\text{salophen})]_2$ (**3**). ^j Sliding mechanism as shown in Scheme 1.

Scheme 2. Overall Reaction Mechanism Including the L Exchange in $\text{UO}_2(\text{salophen})\text{L}$ (**1**, **2**; eq 12), the Formation of $[\text{UO}_2(\text{salophen})]_2$ (**3**) from Complexes **1** and **2** (eq 1), and the Enantiomer Exchange of Complex **3** (Scheme 1)



no longer independent of eq 1. On the other hand, in Figures 5 and S5, the azomethine signals of $\text{UO}_2(\text{salophen})\text{L}$ and **3** were separated in all temperature ranges despite the NMR line-broadening phenomena due to the L-exchange reaction in $\text{UO}_2(\text{salophen})\text{L}$ and the enantiomer exchange of **3**. This means that the reaction rate of eq 1 is much slower than those of the reactions depicted in eq 12 and Scheme 1, i.e., eq 1 seems to be independent of these reactions. Consequently, it can be considered that the $\text{UO}_2(\text{salophen})$ fragments in complex **3** are combined even in the process of its enantiomer exchange as shown in Scheme 1. It was difficult to perform kinetic analysis for the enantiomer exchange of **3** in CD_2Cl_2 (Figure 11a), because the multiplet phenyl signals of **3** were very complicated and the NMR signals due to the azomethine groups nearer to and farther from the bridging phenoxide unexpectedly overlapped in Figure 11a

despite their different chemical environments as described in section 3.2.

In CDCl_3 (Figure 11b), two signals due to the azomethine group of complex **3** can be observed at 9.59 and 9.56 ppm at 213 K, which is comparable to the results of Figure S5. In contrast to the CD_2Cl_2 system, these azomethine signals at low temperature broadened and finally coalesced into one peak with increasing temperature, as shown in the inset of Figure 11b.⁴⁴ This phenomenon indicates the occurrence of enantiomer exchange of **3** shown in Scheme 1. All other spectral features of Figure 11b were same as those in the CD_2Cl_2 system (Figure 11a).

As seen from the inset of Figure 11b, both azomethine signals shifted to higher field with increasing temperature. This leads to difficulty in the kinetic analysis for the enantiomer exchange of **3** (Scheme 1) using the spectral

simulation of the azomethine signals. However, in the temperature range of so-called slow-exchange limit,^{34,35} the first-order rate constant of the enantiomer exchange of **3** (k_{ex}) can be estimated from the line width of the azomethine signals. In Figure 11b, this limit was applicable to the temperature range from 248 to 263 K. The k_{ex} values calculated from the line widths at 248, 253, 258, and 263 K were 0.4, 0.9, 1.8, and 2.9 s⁻¹, respectively. From the best fit of eq 15 to the estimated k_{ex} values,⁴⁷ the activation parameters of Scheme 1 were obtained as $\Delta H_{\text{ex}}^{\ddagger} = 61 \pm 6$ kJ·mol⁻¹ and $\Delta S_{\text{ex}}^{\ddagger} = -3 \pm 24$ J·mol⁻¹·K⁻¹. Although the estimation of these activation parameters, especially for $\Delta S_{\text{ex}}^{\ddagger}$, is rough, the k_{ex} value at 298 K could be calculated as 87 s⁻¹ by eq 15.

Consequently, the overall reaction mechanism in Scheme 2 is proposed on the basis of the information concerning the L-exchange reactions in UO₂(salophen)L through the dissociative and associative paths, the formation of **3** from UO₂(salophen)L via the intermediate UO₂(salophen), and the enantiomer exchange of **3** by the sliding motion of the UO₂(salophen) fragments. The thermodynamic and kinetic data for the reactivity of these uranyl-salophen complexes are summarized in Table 5.

4. Conclusion

In this study, we have investigated the molecular structures of the uranyl-salophen complexes, UO₂(salophen)DMF (**1**), UO₂(salophen)DMSO (**2**), and that without any unidentate ligands (L). As a result, the uranyl-salophen complex without L was identified as the dimeric compound, [UO₂(salophen)]₂ (**3**), in which the UO₂(salophen) fragments are held together by the coordination from one of the oxygen atoms in the phenoxides in salophen to the fifth equatorial coordination site of the other UO₂(salophen). Furthermore, it was demonstrated by UV-visible absorption spectroscopy that complex **3** keeps its dimeric structure even in solutions of the noncoordinating solvents such as CH₂Cl₂ and CHCl₃ and is equilibrated with UO₂(salophen)L upon addition of

free L. The equilibrium constants and formation enthalpy and entropy of the equilibrium between UO₂(salophen)L and **3** (eq 1) were evaluated from UV-visible and ¹H NMR spectral changes. These thermodynamic parameters suggested differences in the coordination abilities of L to UO₂(salophen) (DMF < DMSO) and the solvent effect on the formation of **3** (CH₂Cl₂ < CHCl₃).

The reactivities of complexes **1–3** were also examined using ¹H NMR spectroscopy. As consequence, it was suggested that the DMF-exchange reaction in **1** proceeds through two pathways, i.e., dissociative and associative, and that the corresponding reaction in **2** occurs only dissociatively. Furthermore, it was proposed that the enantiomer exchange of complex **3** passes through the sliding motion of the UO₂(salophen) fragments rather than the flipping motion of the distorted salophen and that the UO₂(salophen) fragments in **3** are combined even throughout the whole process of enantiomer exchange. In conclusion, we proposed Scheme 2 as the overall reaction mechanism on the basis of the information concerning the reactivity of the complexes **1–3**.

Acknowledgment. We thank Prof. Kunihiro Mizumachi for helpful discussions.

Supporting Information Available: IR spectra of UO₂(salophen)DMF (**1**), UO₂(salophen)DMSO (**2**), and [UO₂(salophen)]₂ (**3**); ¹H NMR spectrum of H₂ salophen in CD₂Cl₂, ¹H NMR spectra of CDCl₃ solutions of UO₂(salophen)L; L concentration dependence of UV-visible absorption spectra corresponding to eq 1; comparisons between the experimental ¹H NMR spectra and spectra simulated using the gNMR program in the kinetic analyses of the L-exchange reactions in UO₂(salophen)L; Eyring plots for k_1 and k_2 of the DMF-exchange reaction in complex **1**; scheme of the flipping model of the enantiomer exchange of complex **3**; and crystallographic information files of UO₂(salophen)DMF·CH₂Cl₂ (**1**·CH₂Cl₂), **2**, **3**, and [UO₂(salophen)]₂·0.5CH₂Cl₂ (**3**·0.5CH₂Cl₂). This material is available free of charge via the Internet at <http://pubs.acs.org>.

IC0611950